Available online at www.sciencedirect.com
SCIENCE DIRECT®
International Journal of Thermal Sciences 44 (2005) 644–655
International Journal of Thermal Sciences
www.elsevier.com/locate/ijts

Numerical heat transfer in a rectangular channel with mounted obstacles on upper and lower walls

Abdelkader Korichi [a], Lounes Oufer [b,*]

[a] *Centre Universitaire de Médéa, Quartier Ain D'heb Médéa 26000, Algeria*
[b] *Université des Sciences et de la Technologie Houari Boumediene, Faculté de Génie Mécanique et de Génie des Procédés, Département de Génie des Procédés, B.P. 32, El-Alia, Bab-Ezzouar, Algiers, Algeria*

Received 10 January 2004; received in revised form 23 October 2004; accepted 3 December 2004

Available online 9 April 2005

Abstract

A numerical investigation of convective heat transfer between a fluid and three physical obstacles (blocks) mounted on the lower wall (2 blocks) and on the upper wall (1 block) of a rectangular channel was conducted. Laminar flow of the fluid circulating through the channel was assumed. The effect of the Reynolds number, block spacing and dimensions and solid to fluid thermal conductivity ratio were studied. A uniform heat flux through the blocks was assumed. The results showed that transition from steady to unsteady flows occurred at lower values of the Reynolds number when an obstacle is placed on the upper wall of the channel. The isotherms around the blocks were presented and the heat transfer evaluated through the Nusselt number. As expected, the results obtained showed that as the value of the Reynolds number was increased, the heat removed from the obstacles increased sensibly with a maximum heat removal around the obstacle corners. Moreover, the temperature difference between the three obstacles decreased as the Reynolds number was increased. Some disagreement in the results was observed when compared with those reported in the literature.

Keywords: Convective heat transfer; Laminar flow; Channel; Obstacle; Numerical solution

1. Introduction

Convective cooling of electronic components mounted on circuit boards has been the subject of a large number of scientific papers in the last decade. This interest was motivated by the rapid advances in electronic technology with the trends of the electronic industry being oriented toward the development of more and more compact and powerful computers. In all circumstances, such an objective may never be attained without an effective removal of the heat released by electronic components under operation.

Literature in that area is quite diverse as many experimental and theoretical studies have been reported. Ortega et al. [1] studied experimentally the conjugate convective and conductive heat transfer for laminar, transitional and turbulent boundary layer flow over a flush-mounted. The authors reported that substrate conduction decreased monotonically with increased Reynolds number. Moreover, heat transfer was found to depend not only on the maximum fluctuating velocity but also on the geometry of the grooved surface. Young and Vafai [2] investigated the forced convective heat transfer of individual and array of multiple two-dimensional obstacles for a Reynolds number ranging from 800 to 1300. The effect of a change in the channel height and input heat power was investigated and an empirical correlation established. In another study, Wang and Vafai [3] studied the mixed convection and pressure losses in a channel with discrete flush-mounted and protruding heat sources. In the same work, the effect of obstacle geometry and flow rate was considered. An empirical correlation for both pressure drop and Nusselt number was presented.

* Corresponding author. Tel./Fax: (+213)21 24 71 69.
E-mail addresses: a_korichi@hotmail.com (A. Korichi), lounesoufer@yahoo.com, loufer@usthb.dz (L. Oufer).

1290-0729/$ – see front matter
doi:10.1016/j.ijthermalsci.2004.12.003

Nomenclature

D_h	hydraulic diameter, $= 2H$	m
h	dimensionless obstacle height, $= h^*/H$	
h^*	obstacle height	m
H	channel height	m
K	thermal conductivity	$W{\cdot}m^{-1}{\cdot}K^{-1}$
L	dimensionless outlet length	
L^*	outlet length	m
L_0	dimensionless inlet length	
L_0^*	inlet length	m
Nu_x	local Nusselt number, $= \frac{-1}{\theta_m}\frac{\partial\theta}{\partial n}\vert_{\text{block surface}}$	
$\overline{Nu_x}$	time averaged local Nusselt number, $= \frac{1}{\tau_p}\int_0^{\tau_p} Nu_X \,\mathrm{d}\tau$	
P	dimensionless pressure, $= p^*/\rho u_{0m}^2$	
p^*	pressure	Pa
Pe	Peclet number	
Pr	Prandtl number	
q''	heat flux	$W{\cdot}m^{-2}$
Re	Reynolds number	
s	dimensionless obstacle spacing, $= s^*/H$	
s^*	obstacle spacing	m
T	temperature	K
T	time	s
u, v	dimensionless velocity components, $= \frac{u^*}{u_{0m}}, = \frac{v^*}{u_{0m}}$	
u^*, v^*	velocity components	$m{\cdot}s^{-1}$
w	dimensionless obstacle width, $= w^*/H$	
w^*	obstacle width	m
x, y	dimensionless coordinates, $= x^*/H, = y^*/H$	
x^*, y^*	physical coordinates	m

Greek symbols

α	thermal diffusivity, $= k/\rho C_p$	$m^2{\cdot}s^{-1}$
θ	dimensionless temperature, $= \frac{T-T_0}{q''H/k}$	
ρ	density	$kg{\cdot}m^{-3}$
ν	kinematic viscosity	$m^2{\cdot}s^{-1}$
τ	dimensionless time, $= tu_{0m}/H$	

Subscripts

cr	critical
f	fluid
m	mean
s	solid
0	inlet
1, 2, 3	refer to obstacle number

Superscript

$*$	dimensional

Garimella and Schiltz [4] studied heat transfer enhancement of cooling by using a protruding heat source and an array of roughness elements and ribs on the opposite wall of a narrow rectangular channel. A Nusselt number correlation was proposed. Jubran et al. [5] carried out an investigation of heat transfer and pressure drop in rectangular channels containing monocubical obstacles. The factors of interest were obstacle dimensions and their shapes. Garimella and Eibeck [6] examined the effect of spanwise spacing on heat transfer from an array of protruding heat sources in forced convection. They concluded that the upper limit of heat transfer was obtained at a ratio of 2.2 of the obstacle height to spanwise spacing. In another study [7], the same authors found that the Nusselt number decreased with an increase in the ratio of channel height to obstacle height, and approached an asymptotic value at the fourth row. Very recently, Meinders and Hanjalic' [8] presented an investigation on the effect of arrangement type of two wall-mounted cubes exposed to turbulent flow. Their results showed a large variation in the distribution of the local convective heat transfer for the various in-line and staggered configurations utilized. Furthermore, the cube-averaged heat transfer coefficients were found to be independent of cube placement.

Numerical studies in that area of research consisting of enhancement of cooling of electronic devices are becoming more and more numerous. Davalath and Bayazitoglu [9], using finite volume formulation, studied forced convection over three block heat sources attached to the lower wall of a channel. They developed a model for prediction of the Nusselt number as a function of the Reynolds and the Prandtl numbers. Using the Gherkin-finite-element formulation, an important work was carried out by Young and Vafai [10,11] who investigated the flow and heat transfer in a rectangular channel containing many heated obstacles mounted on its lower wall. The dependence of the flow and temperature fields on parametric changes such as the Reynolds number, solid thermal conductivity, geometric parameters and heating method was studied. The results were presented in the form of correlations established for one and for arrays of multiple heated obstacles.

Moreover, in much of the recently reported work, researchers showed a strong interest in enhancement of heat transfer from electronic components by passive cooling. For instance, Wu and Perng [12] investigated the effect of installing an oblique plate on heat transfer over an array of five obstacles mounted in a horizontal channel. They observed an enhancement of heat transfer represented by an increase in the value of the Nusselt number of up to 39.5%. Sultan [13] carried out an experimental study on the effect of open holes ratio on the mean heat transfer coefficient from three protruding mounted blocks simulating electronic components. The results showed an increase in the amount of heat trans-

fer by about 31% in the value of the Nusselt number. The same technique was used by Leung et al. [14] for Reynolds numbers ranging from 500 to 19 000. They obtained an increase in heat transfer of up to 130%.

Rachedi and Chikh [15] studied the effect of insertion of porous media to enhance heat transfer from three mounted surfaces on a wall. The main result presented was a maximum decrease of the temperature of the surfaces of about 15%. Jubran et al. [16] looked at the convective heat transfer and pressure drop over an array of surfaces of both rectangular and squared surfaces. Their results showed that the use of individual rectangular modules enhanced heat transfer more than square modules. Implementation of cylindrical modules in the middle of an array was also found to enhance heat transfer quite sensibly. Finally, Herman and Kang [17] studied the effect of placement of curved vanes in a grooved channel. Enhancement of heat transfer was attained with rates comparable to those obtained in turbulent flow although at low Reynolds numbers. This enhancement of heat transfer was mainly the result of fluid flow acceleration between the vane and the heated block and the elimination of large recirculation regions in the grooves.

The present work represents a two-dimensional numerical investigation of forced laminar convection in a rectangular channel containing three heated obstacles: two attached to the lower wall and one to the upper wall of the channel, all placed alternatively. The purpose is to quantify the influence of alternating the placement of the blocks between the upper and the lower walls. The effect of different geometric configuration and flow parameters on the conjugate heat transfer and flow field are also explored.

2. Mathematical formulation

The physical geometry considered in this study is shown in Fig. 1. The flow is assumed to be laminar and incompressible. The fluid is viscous Newtonian and buoyancy induced effects are assumed negligible. All the physical properties of the fluid and of the solid are considered constant. The Prandtl number is taken equal to 0.71. The dimensionless groups defined in the nomenclature are used to express the governing transport equations in the dimensionless form. The resulting non-dimensional equations for mass, momentum and energy conservation are presented in the Cartesian coordinate system as follows:

Mass:

$$\frac{\partial u}{\partial x}+\frac{\partial v}{\partial y}=0 \tag{1}$$

x-momentum:

$$\frac{\partial u}{\partial \tau}+u\frac{\partial u}{\partial x}+v\frac{\partial u}{\partial y}=-\frac{\partial p}{\partial x}+\frac{1}{Re}\left(\frac{\partial^2 u}{\partial x^2}+\frac{\partial^2 u}{\partial y^2}\right) \tag{2}$$

y-momentum:

$$\frac{\partial v}{\partial \tau}+u\frac{\partial v}{\partial x}+v\frac{\partial v}{\partial y}=-\frac{\partial p}{\partial y}+\frac{1}{Re}\left(\frac{\partial^2 v}{\partial x^2}+\frac{\partial^2 v}{\partial y^2}\right) \tag{3}$$

Energy:

For the fluid phase:

$$\frac{\partial \theta_f}{\partial \tau}+u\frac{\partial \theta_f}{\partial x}+v\frac{\partial \theta_f}{\partial y}=\frac{1}{Pe}\left(\frac{\partial^2 \theta_f}{\partial x^2}+\frac{\partial^2 \theta_f}{\partial y^2}\right) \tag{4}$$

For the solid phase:

$$\frac{\partial \theta_s}{\partial \tau}=\frac{\alpha_s}{\alpha_f}\left(\frac{\partial^2 \theta_s}{\partial x^2}+\frac{\partial^2 \theta_s}{\partial y^2}\right) \tag{5}$$

Boundary conditions:

At the inlet, the flow is fully developed with a parabolic profile $u_0(y)=6y(1-y)$. The upstream face of the first obstacle is located at $L_{\text{in}}=6.0$. Such distance is chosen to ensure that the inlet length has no effect on the results. The temperature at the first obstacle surface for different L_{in} values is shown in Fig. 2(a). At the outlet, all gradients are assumed to be zero. The downstream length, L_{out} , is considered significantly long to ensure that the recirculation zone is inside the computational domain and the outflow has no effect upon the physical variables investigated. A value of $L_{\text{out}}=23$ is found to be sufficient. The temperature at the last obstacle surface for different L_{out} values is shown in Fig. 2(b). At the channel walls ($y=0,\ y=1$), the no-slip condition is assumed, that is $u=v=0$.

For the thermal boundary conditions, the walls are assumed to be insulated except at the obstacle bases where a dimensionless heat flux value of unity is imposed (i.e.,

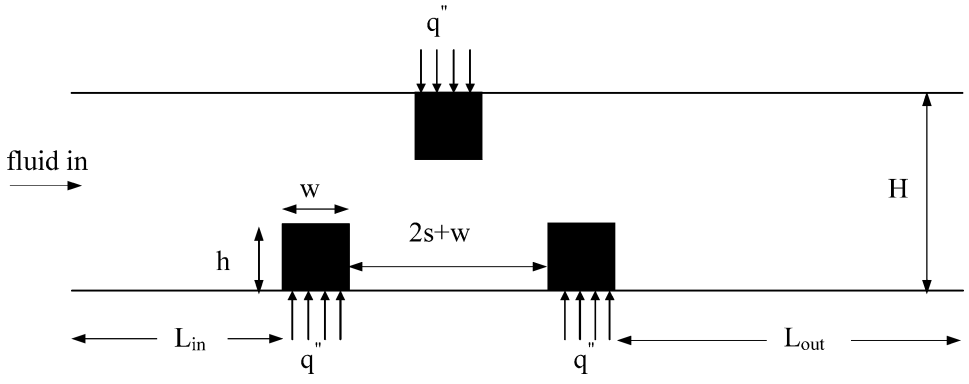

Fig. 1. Schematic diagram of the flow and geometrical configuration.

$q'' = 1$). This allows us to calculate the real dimensional temperature at any position by multiplication with the given heat flux input since, $T = \theta \frac{q''H}{k_f} + T_0$. At the solid–fluid interface, continuity of the heat flux and of the temperature is also assumed.

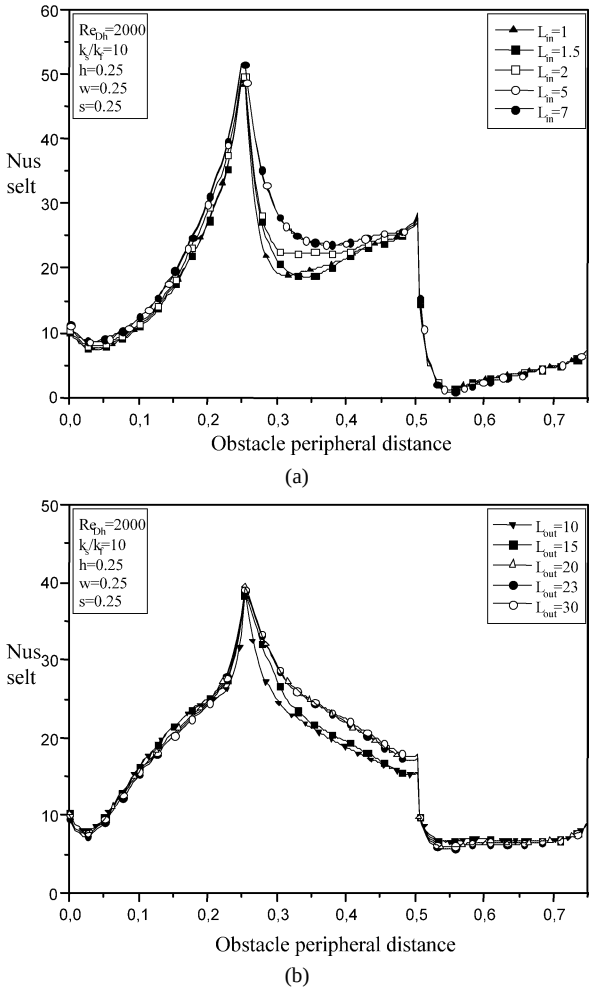

Fig. 2. Effect of channel inlet and outlet lengths on obstacle surface temperature: (a) Effect of L_{in} on the surface temperature of the first obstacle; (b) Effect of L_{out} on the surface temperature of the last obstacle.

3. Numerical solution

The governing transport equations associated with the boundary conditions were solved using the finite volume formulation. The SIMPLER algorithm developed by Patankar [18] is adopted. The time discretization scheme is implicit with second order accuracy. For the spatial discretization the central second order differencing scheme is used for the diffusive terms and the second order upwind scheme is used for the convective terms. The iterative solution is continued until the residuals for all computational cells became less than 10^{-6} for all dependent variables. The grid is non uniform and is highly concentrated close to the obstacle to capture high gradient velocity, pressure and temperature. In order to ensure grid independence of the results, a series of tests for non uniform grids were carried out. The obtained

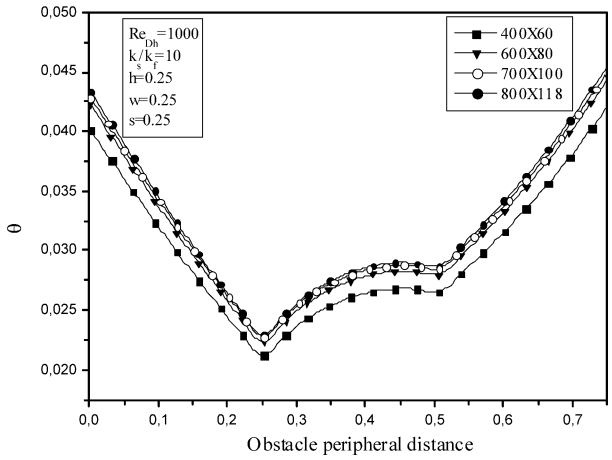

Fig. 3. Comparison of the obstacle surface temperature for various mesh values.

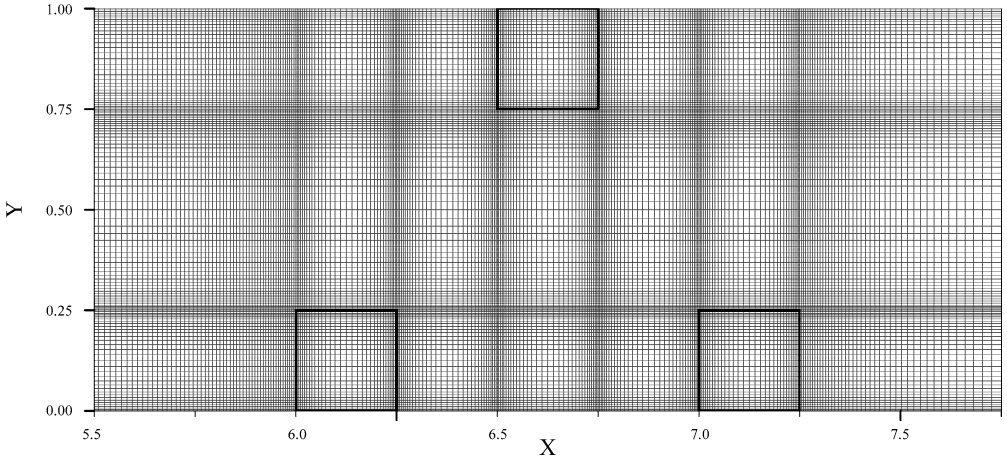

Fig. 4. Representation of the grid distribution in the channel.

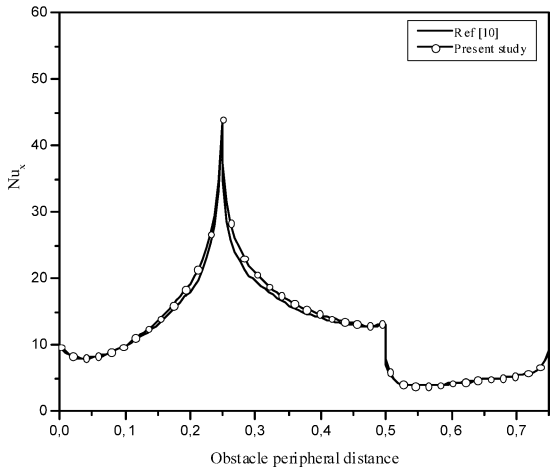

Fig. 5. Validation plot of the present numerical simulation by comparison with the results of Young and Vafai [10].

results are plotted in Fig. 3. The choice of the grid distribution (800×118) is found to be sufficient for the range of Reynolds numbers investigated. The number of nodes distributed over the length of obstacle face for the base line configuration is equal to 32. The grid distribution for this configuration is shown in Fig. 4. For unsteady flow, the time marching calculations were started with the fluid at rest and constant dimensionless time step of 0.001.

In treatment of the solid–fluid interface a domain extension method is applied the details of which are largely presented by Chen and Han [19]. Validation of the numerical simulation was attained by performing calculations for the case of laminar flow with one obstacle attached to the lower wall, case for which the results exist in the literature. Fig. 5 compares the results of the present work with those of Young and Vafai [10] for the same conditions. A quite good agreement is observed between the two studies. At this point, it is to be mentioned that no comparison with experimental data is performed herein simply because in our knowledge no such results are available in the literature for local heat transfer and similar geometrical systems.

4. Results and discussion

The dimensionless parameters that must be specified and which characterise the flow field and heat transfer are the Reynolds number based on the hydraulic diameter, Re_{D_h} ($D_h = 2H$), the obstacles dimensions, h, w and s, and the thermal conductivity ratio, k_s/k_f.

The Reynolds number is varied from 400 to 2000 for the baseline configuration ($h = w = s = 0.25$), and $k_s/k_f = 10$. The effect of thermal conductivity ratio is investigated in the range 10 to 1000 for $Re_{D_h} = 800$ and baseline configuration. For the effect of obstacles dimensions, the Reynolds number and thermal conductivity ratio are taken equal to 800 and 10, respectively. By considering the time evolution of the flow and thermal fields in the range of Reynolds number from 400 to 2000, it was found that the transition from steady to unsteady flow occurs at low Reynolds number when compared to the channel with no obstacle on the upper wall. For a grooved channel, Herman and Kang [17] found that the flow transition occurred in the Reynolds number range of 1050 to 1300. Similar findings were also reported in the case of an oblique plate [12].

Table 1
Critical values of Reynolds number for various obstacle dimensions

Configuration	$Re_{D_{h\mathrm{cr}}}$
Case 1: $h = w = s = 0.25$	~ 920
Case 2: $h = s = 0.25$; $w = 0.125$	~ 740
Case 3: $h = 0.125$; $w = s = 0.25$	> 2000
Case 4: $h = w = 0.25$; $s = 0.125$	~ 910
Case 5: $h = 0.5$; $w = s = 0.25$	~ 280

The critical Reynolds number $Re_{D_{h\mathrm{cr}}}$ depends on obstacle dimensions and spacing. In this study it is observed that $Re_{D_{h\mathrm{cr}}}$ is highly affected by the obstacle height, h. Table 1 summarises values of $Re_{D_{h\mathrm{cr}}}$ for the various configurations considered in this study. The time-averaged dimensionless temperature and velocity components are calculated in the interval containing several flow cycles of vortex shedding. For a better understanding of the phenomena around the heated obstacles, only the flow and thermal fields close to the heated obstacles are presented in all figures.

To illustrate the effect of modification of the flow pattern by placing obstacles in both upper and lower walls, a calculation is performed for two obstacles placed in the lower wall. Fig. 6 shows streamlines for flow in a channel containing two obstacles attached to the lower wall. It appears that without any obstacle on the upper wall, the streamlines begin to deflect upstream of the first obstacle. A clockwise vortex is generated upstream near the first obstacle. As the fluid turns upward into the bypass passage between the top face of the first obstacle and the upper channel wall, the fluid directly impinges the top face of the second obstacle causing a recirculation zone to be formed within the interobstacle groove. A third and more important clockwise vortex is also created downstream of the last obstacle. It is noticed that each obstacle is cooled more than the adjacent one placed downstream by about 31%. Moreover, using obstacles on both the upper and lower walls, counterclockwise vortices are developed upstream and downstream of the upper wall obstacle. The fluid flows upward into the narrow space between the obstacles on the lower and upper walls with a quite drastic acceleration. As a result, the recirculation zones become shorter and more intense except for the last recirculating zone. The vortex in interobstacle groove is seen to be the most affected. The fluid flow then interacts more with the obstacle faces as illustrated by Fig. 7(a) which shows the streamlines for $Re_{D_h} = 400$ and for a baseline configuration $h = w = s = 0.25$. It is observed that the flow tends to enter in-between obstacle cavities. For higher values of the Reynolds number (Fig. 7(b) and (c)), the flow becomes unsteady periodic and the length of the recirculation zone

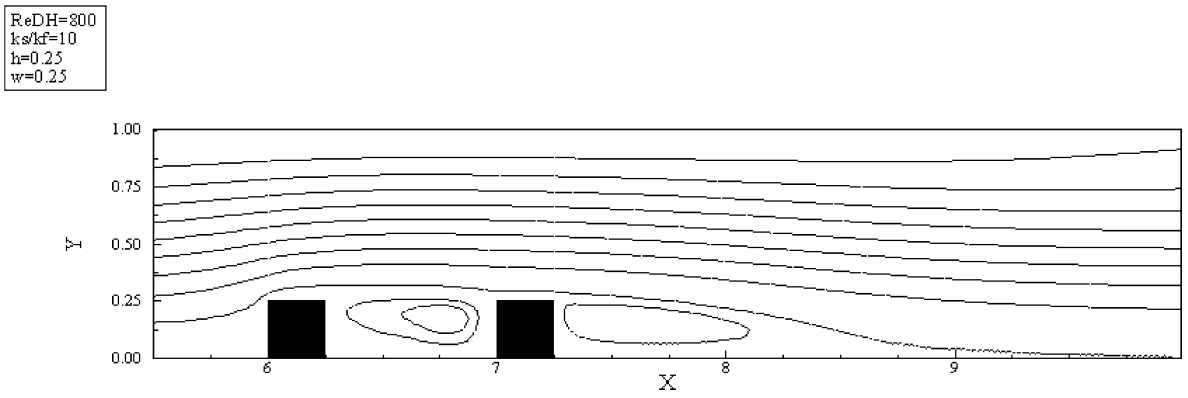

Fig. 6. Streamlines obtained in the absence of an obstacle on the upper wall.

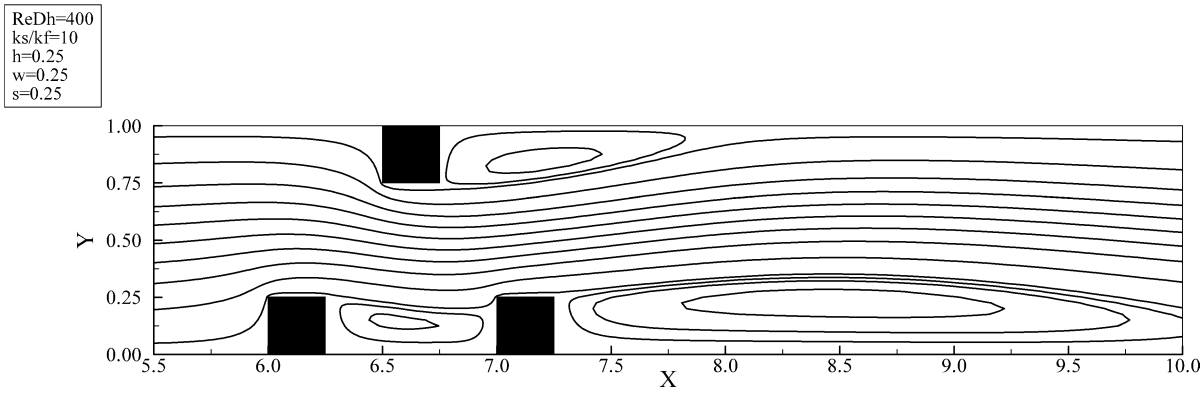

(a)

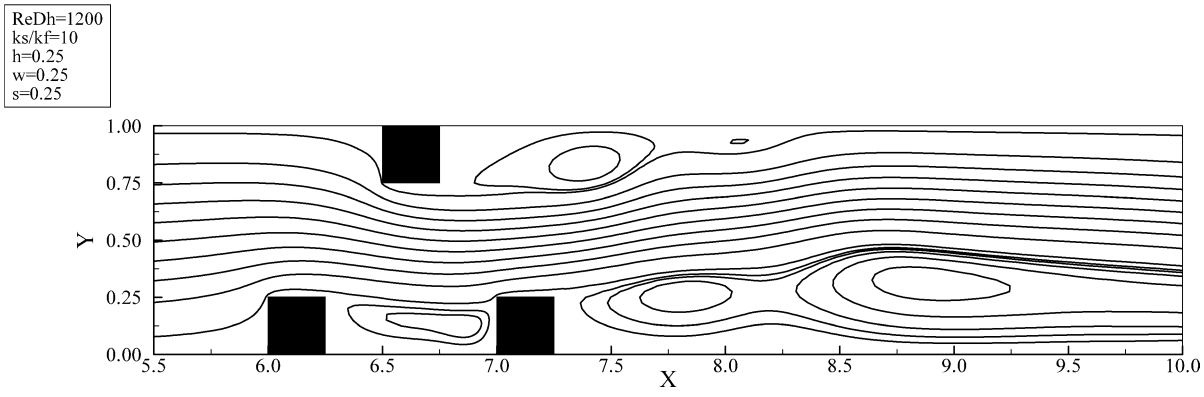

(b)

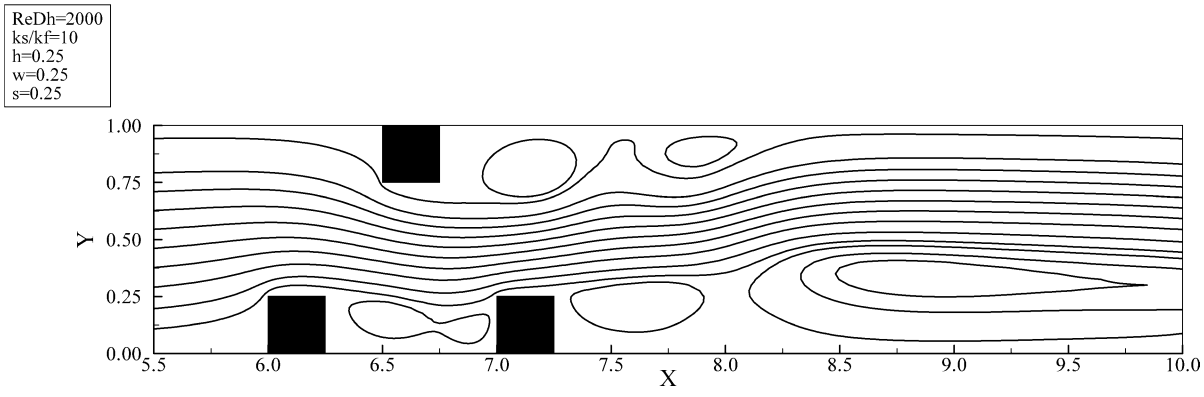

(c)

Fig. 7. Time-averaged streamlines for $k_s/k_f = 10$, $h = w = 0.25 = 0.25$ and for: (a) $Re = 400$; (b) $Re = 1200$; (c) $Re = 2000$.

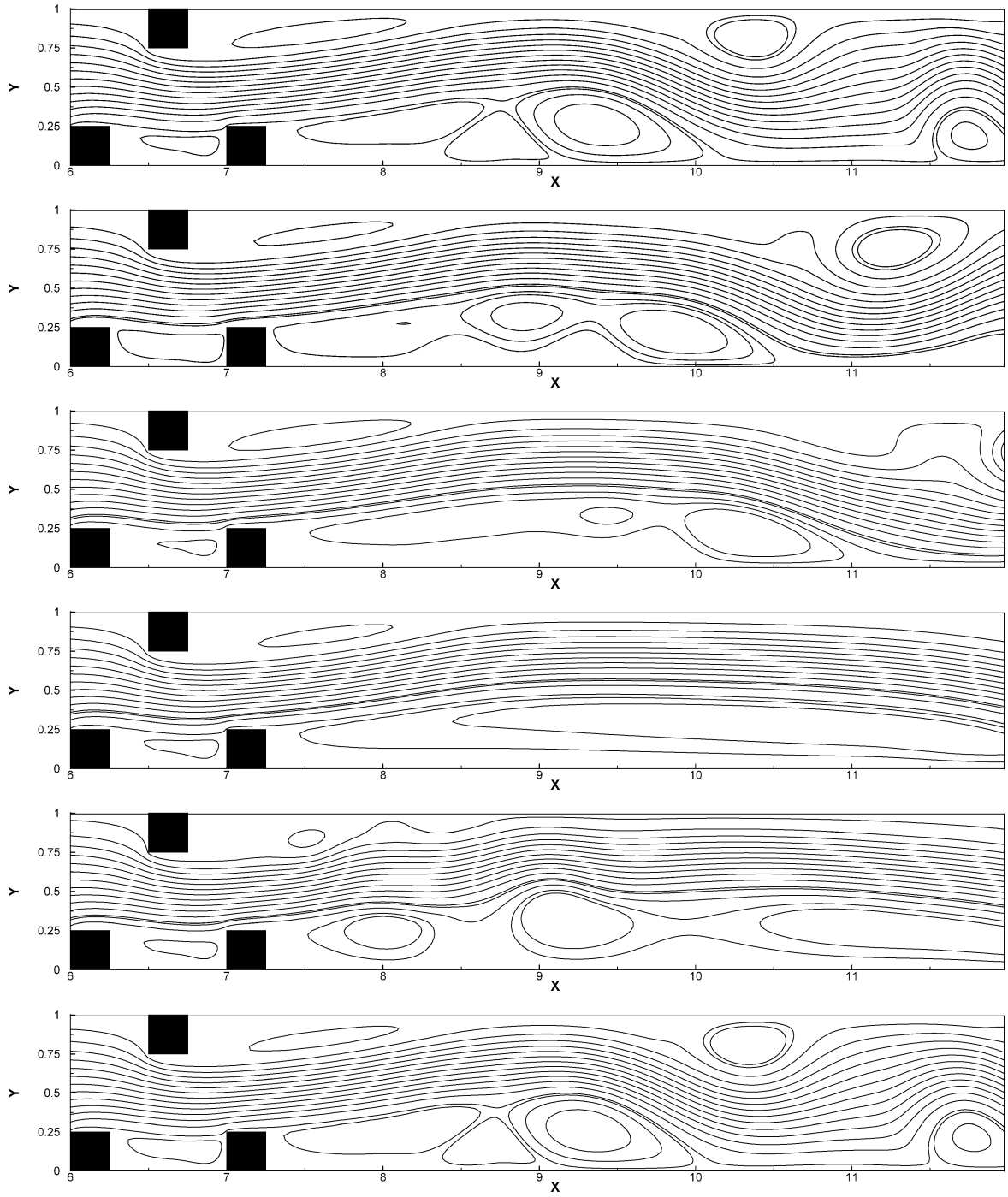

Fig. 8. Streamlines per cycle of vortex shedding at $Re = 1200$ and $h = w = s = 0.25$.

seems to get reduced when compared with the configuration without obstacle on the upper wall. Besides, the recirculation zone behind the last obstacle is more pronounced. In the transition from steady to unsteady periodic flows, a wave is induced by vortex shedding behind the last obstacle. This wave results in a change of the recirculating zone behind the latter. Fig. 8 shows instantaneous streamlines for five time intervals within one period of oscillation. This phenomenon is similar to that obtained by employing an oblique plate over an arrangement of obstacles [13] in which the streamlines present a wavy form at the end of the array. It is clear that unsteadiness seems more pronounced as Reynolds number increases.

The representation of the time-averaged isotherm contours obtained for different values of the Reynolds number is shown in Fig. 9. It is observed that the isotherm lines are denser close to the upstream and the top faces of the obstacles. Furthermore, the isotherm contours near the down-

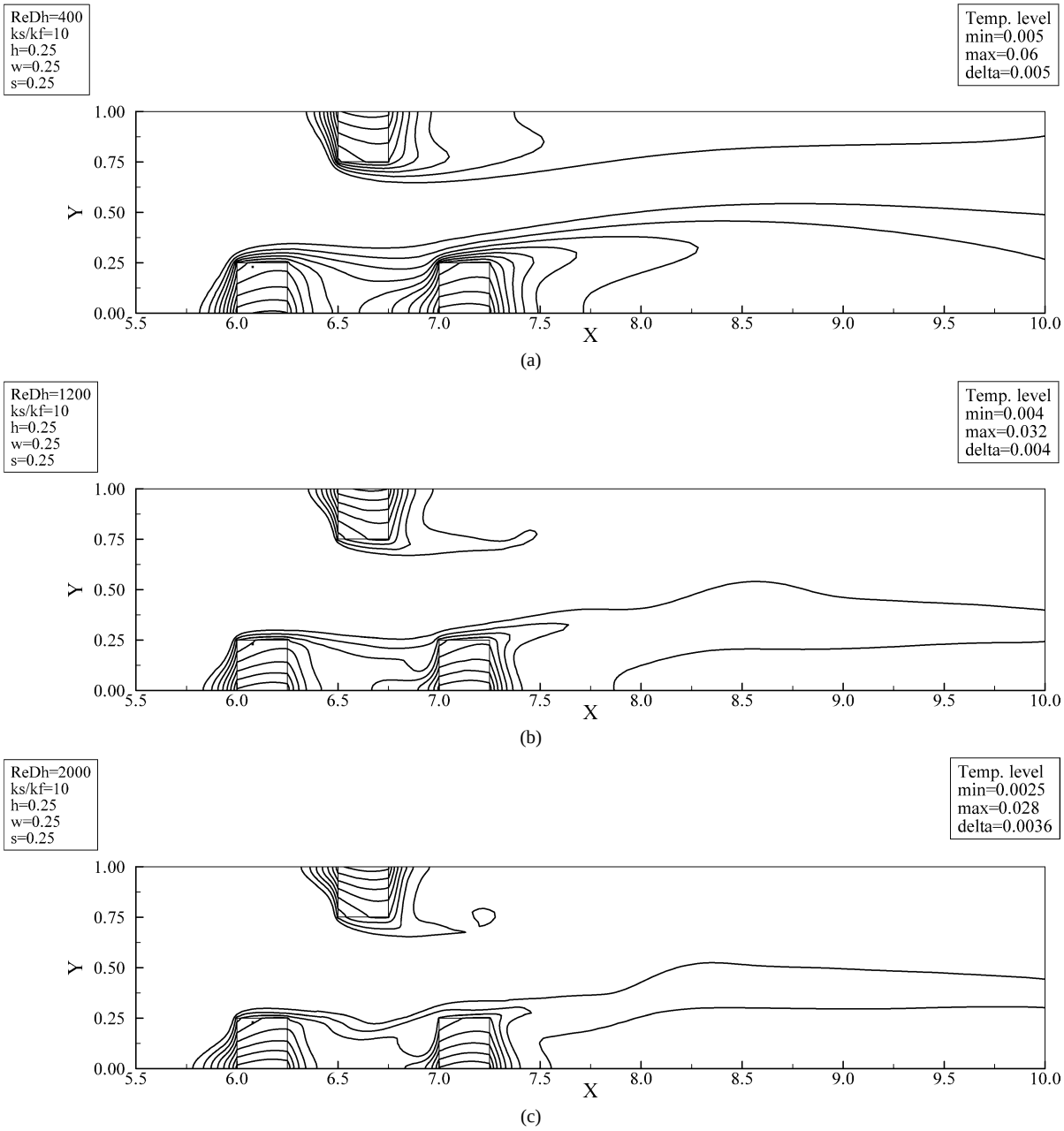

Fig. 9. Time-averaged isotherms for $k_s/k_f = 10$, $h = w = s = 0.25$ and for: (a) $Re = 400$; (b) $Re = 1200$; (c) $Re = 2000$.

stream face of the obstacles are denser than those obtained in channels without obstacle on the upper wall. The latter results are not presented here for conciseness but if needed, the reader may consult the related references [9,11]. It is also observed that when the Reynolds number increases, a vortex appears inside the inter-obstacle cavities and the isotherm contours become thoroughly denser especially near the faces. This yields to the removal of higher quantities of energy from both the right and the left obstacle faces.

In Figs. 10 and 11 is represented the time-averaged dimensionless temperature of the obstacle surfaces as a function of the obstacle peripheral distance and as a function of the dimensionless channel distance, respectively. First, It can be noticed that the temperature difference between the first and the third obstacle decreases with increasing Reynolds number, in contrast with the case where no obstacle is present on the upper wall. The time-averaged temperature of obstacle surface for $Re_{D_h} \leqslant 1200$ shown in Fig. 10 indicates that the surface temperature profile around the first obstacle is located below that of the third one, and the temperature of the second is even lower than the two. This may be explained by the fact that the first obstacle situated in the free stream causes a very weak clockwise vortex to form forward to the upward lower corner as was discussed elsewhere [11]. For the second obstacle the flow is redirected by the top of the first obstacle which then removes more energy from his

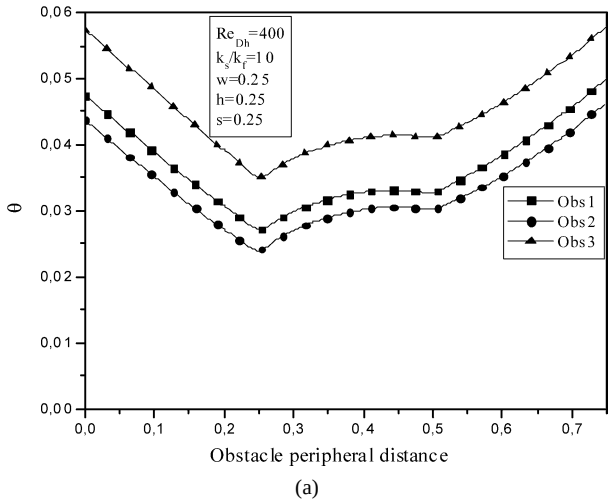

(a)

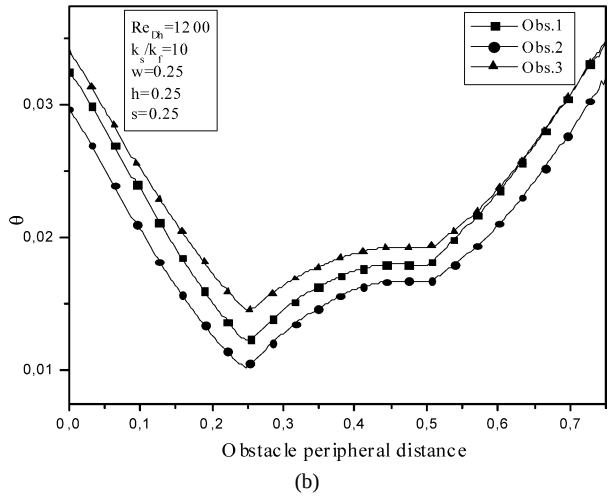

(b)

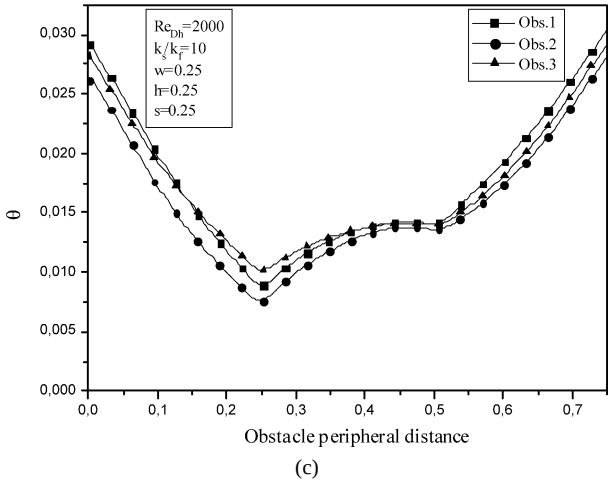

(c)

Fig. 10. Time-averaged temperature at the surface of the three obstacles for $k_s/k_f = 10$, $h = w = s = 0.25$ and for: (a) $Re = 400$; (b) $Re = 1200$; (c) $Re = 2000$.

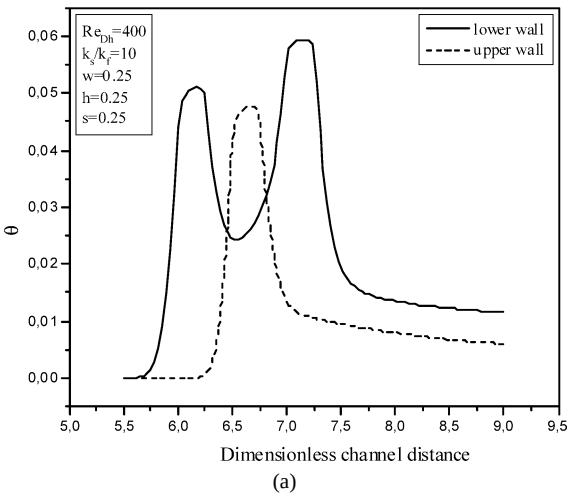

(a)

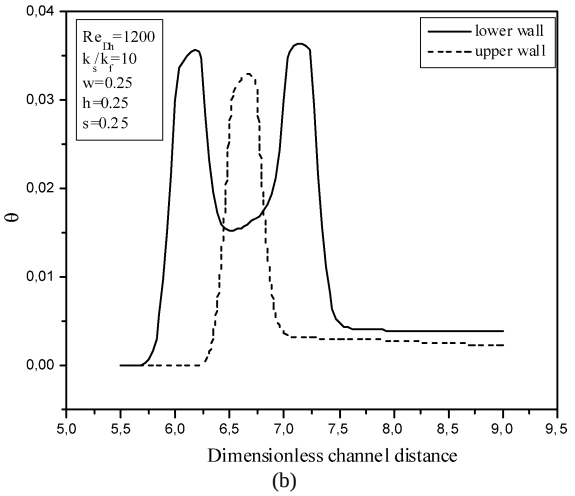

(b)

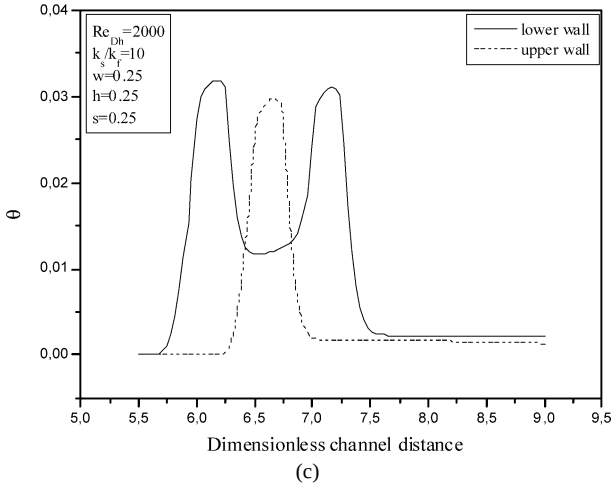

(c)

Fig. 11. Time-averaged temperature at the inner surface channel walls for $k_s/k_f = 10$, $h = w = s = 0.25$ and for: (a) $Re = 400$; (b) $Re = 1200$; (c) $Re = 2000$.

first corner. At higher values of the Reynolds number the strength of the redirected flow to the third obstacle is less. As a result, the temperature for the three obstacles becomes nearly the same. In that situation, the flow mix well with the obstacle bases and therefore higher quantities of heat may be removed from the obstacles by the fluid. Fig. 11 presents the lower and upper isolated time-averaged wall temperature profiles for different values of the Reynolds number along the channel distance. The results agree well with those previously presented in the plots of Fig. 10. It is important to

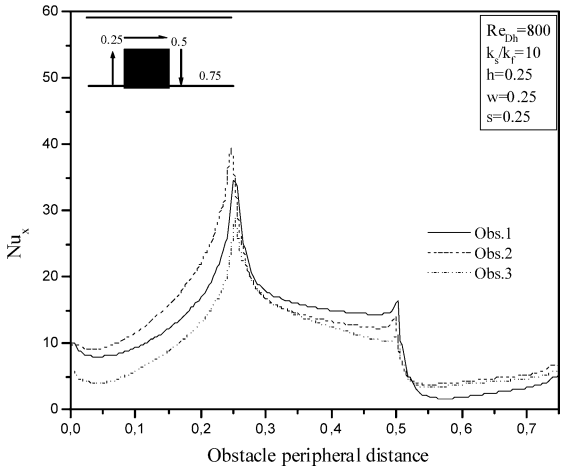

Fig. 12. Variation of the local Nusselt number along the peripheral distance for the three obstacles for $k_s/k_f = 10$, $h = w = s = 0.25$ and $Re = 800$.

mention that the temperature of the wall is the maximum temperature of the component because the temperature distribution in the component is such that it decreases from the wall to the edge of the component.

The heat transfer rate characterised by the value of the Nusselt number calculated for the three obstacles is presented in Fig. 12 as a function of the obstacle peripheral distance for $Re_{D_h} = 800$. All three curves show a peak value at the corner of each obstacle. Moreover, Fig. 13 represents the time-averaged Nusselt number obtained for each of the three obstacles but for values of the Reynolds number equal to 400, 1200 and 2000. As expected, it can be clearly observed that values of the Nusselt number become higher with increasing values in the Reynolds number. For relatively large values of the latter ($Re_{D_h} > 1000$), the Nusselt number curve for the left face of the third obstacle present a local maximum in the face distance. It is believed that such a phenomenon is the result of flow redirection toward the opposite wall by the obstacle. The value of the Nusselt number at the right face of the first and of the third obstacle is nearly constant and has always a positive value. Such an observation seems to be opposite to that previously mentioned in the case of a configuration composed of an array of obstacles in the lower wall [11]. For the first obstacle, the horizontal face is the most affected by the Reynolds number while for the second one, the value of the Nusselt number at the horizontal face decreases with increasing Reynolds number because of the sudden deflection of the flow at the obstacle corner.

The time-averaged overall Nusselt number for the three obstacles is shown in Fig. 14. For a low value of Reynolds number (< 1200), the Nusselt number for the second obstacle is greater than that of the first which itself is greater than that of the third ($Nu_{m2} > Nu_{m1} > Nu_{m3}$). At high Reynolds number values, the time-averaged overall Nusselt number for the first obstacle becomes nearly equal to that for the second one. For the other obstacles and for high Reynolds numbers, the flow redirected by the obstacle situated at the opposite wall mix well the surface obstacle.

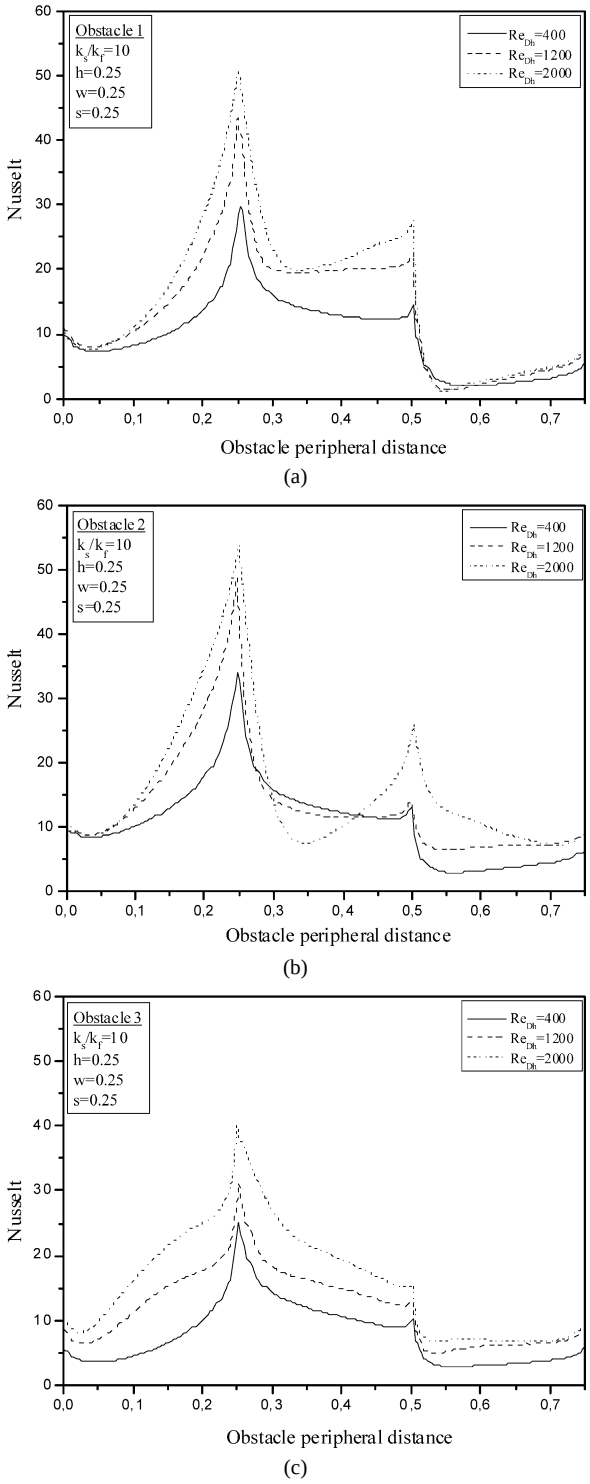

Fig. 13. Effect of Reynolds number on the time-averaged local Nusselt number for $k_s/k_f = 10$, $h = w = s = 0.25$ and for obstacle 1(a), 2(b), 3(c).

The effect of thermal conductivity ratio (k_s/k_f) on heat transfer from the three obstacles is treated in Fig. 15. The results obtained agree well with those reported by Young and Vafai [10,11]. As the thermal conductivity ratio increases, the conductive flux in the solid phase encounters less thermal

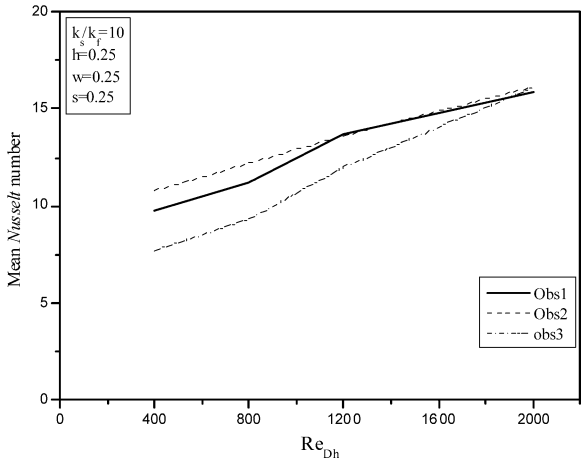

Fig. 14. Variation of the time-averaged overall Nusselt number with Reynolds number for the three obstacles, $k_s/k_f = 10$ and $h = w = s = 0.25$.

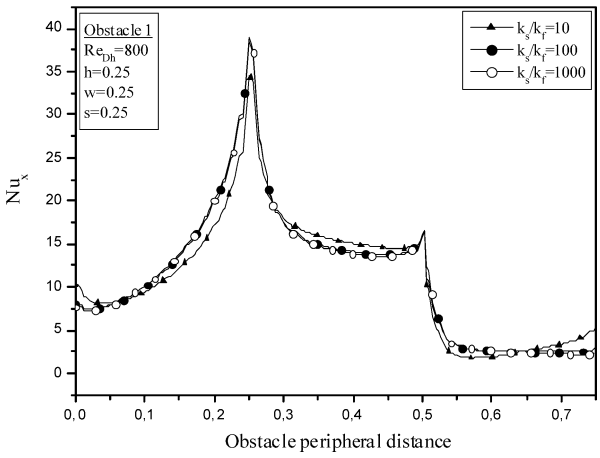

Fig. 15. Effect of the thermal conductivity ratio on heat transfer for the first obstacle and for $h = w = s = 0.25$.

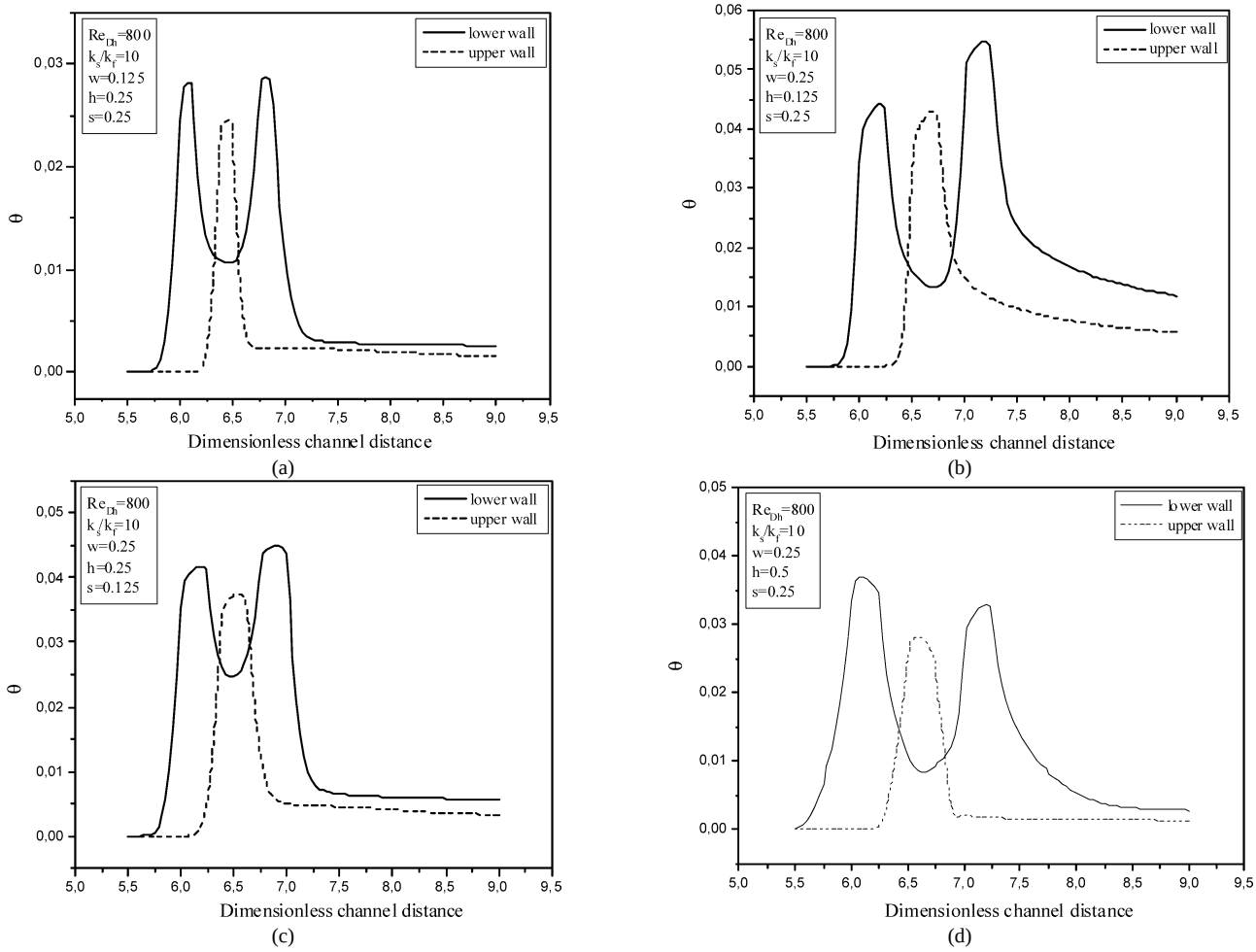

Fig. 16. Time-averaged temperature of channel walls for $k_s/k_f = 10$, $Re = 800$ and for: (a) $h = s = 0.25$, $w = 0.125$; (b) $w = s = 0.25$, $h = 0.125$; (c) $h = w = 0.25$, $s = 0.125$; (d) $w = s = 0.25$, $h = 0.5$.

resistance and as a result and for $k_s/k_f \geqslant 1000$, the solid phase becomes nearly isotherm.

Finally, Fig. 16 shows the time-averaged temperature profile of the isolated upper and lower walls for different obstacle geometries. The minimum obstacle base temperature with respect to obstacle width is obtained for $w = 0.125$ as this corresponds to the minimum input heat flux to the obstacle base. For obstacle heights $h = 0.125, 0.25$ and 0.5,

the minimum temperature is obtained at $h = 0.5$ which corresponds to the maximum exchange surface for the same input heat flux. Besides, a higher obstacle accelerates further the fluid flow and therefore more heat gets removed by the fluid. Moreover, the obstacle spacing seems to have no significant effect as opposed to the case of an array of obstacles placed in the same wall [10,11]. A possible explanation of such findings is that for lower spacing, the flow interacts well with the vertical obstacle face, and larger spacings offer more heat diffusion into the fluid before its contact with the obstacle surface situated downstream.

5. Conclusion

A study of heat transfer and fluid flow in a horizontal channel containing two obstacles on the lower wall and one obstacle on the upper wall located in between the two was conducted. The various parameters investigated were the Reynolds number, the thermal conductivity ratio between the solid and the fluid and the obstacle dimensions. All three obstacles were assumed to be heated with a uniform heat flux which simulates the heat to be generated by electronic components.

The study first showed that when an obstacle is added on the upper wall of the channel, the transition from steady to unsteady flow is obtained at lower values of the Reynolds number. The various isotherms and Nusselt number curves were presented. The results obtained showed that as the value of the Reynolds number was increased, the heat removed from the obstacles increased sensibly with a maximum heat removal around the obstacle corners. Moreover, the temperature difference between the three obstacles decreases as the Reynolds number is increased. It has to be mentioned that some of the results obtained did not agree with those reported previously in the literature for the case of an array of obstacles placed on the lower wall.

Vortex shedding generated by the obstacle on the upper wall can additionally enhance heat transfer along the obstacle surfaces. The wavy flow significantively changes the recirculating zone behind the last obstacle.

The study also showed the same findings as previously reported by other authors concerning the effect of the solid to fluid thermal conductivity ratio. Finally, changing the obstacle dimensions seemed to reduce to changing the heat transfer surface between the solid and the fluid in the sense that higher heat transfer is obtained for higher obstacle dimensions.

References

[1] A. Ortega, U.S. Writh, S.J. Kim, Conjugate forced convection from discrete heat source on a plane conducting surface: A benchmark experiment, in: Heat Transfer in Electronic Systems, in: HDT, vol. 292, ASME, 1994, pp. 25–36.
[2] T.J. Young, K. Vafai, Experimental and numerical investigation of forced convective characteristics of array of channel mounted obstacles, ASME J. Heat Transfer 121 (1999) 34–42.
[3] Y. Wang, K. Vafai, Heat transfer and pressure loss characterisation in a channel with discrete flush-mounted and protruding heat sources, Experimental Heat Transfer 12 (1999) 1–16.
[4] S.V. Garimella, D.J. Schiltz, Heat transfer enhancement in narrow channels using two and three-dimensional mixing devices, ASME J. Heat Transfer 117 (1995) 590–596.
[5] B.A. Jubran, A.S. Al-Salaymeh, Thermal wakes measurement in electronic modules in the presence of heat transfer enhancement devices, Appl. Thermal Engrg. 19 (1999) 1081–1096.
[6] S.V. Garimella, P.A. Eibeck, Effect of spanwise on the heat transfer from an array of protruding elements in forced convection, Internat. J. Heat Mass Transfer 34 (1991) 2427–2430.
[7] S.V. Garimella, P.A. Eibeck, Heat transfer characteristics of an array of protruding elements in single phase forced convection, Internat. J. Heat Mass Transfer 33 (1990) 2659–2669.
[8] E.R. Meinders, K. Hanjalic', Experimental heat transfer from in-line and staggered configurations of two wall-mounted cubes, Internat. J. Heat Mass Transfer 45 (2002) 465–482.
[9] J. Davalath, Y. Bayazitoglu, Forced convection cooling across rectangular blocks, ASME J. Heat Transfer 109 (1987) 321–328.
[10] T.J. Young, K. Vafai, Convective cooling of heated obstacle in channel, Internat. J. Heat Mass Transfer 41 (1998) 3131–3148.
[11] T.J. Young, K. Vafai, Convective flow and heat transfer in channel containing multiple heated obstacles, Internat. J. Heat Mass Transfer 41 (1998) 3279–3298.
[12] H.W. Wu, S.W. Perng, Effect of an oblique plate on the heat Transfer enhancement of mixed convection over heated blocks in horizontal channel, Internat. J. Heat Mass Transfer 42 (1999) 1217–1235.
[13] G.I. Sultan, Enhancing forced convection heat transfer from multiple protruding heat sources simulating electronic components in horizontal channel by passive cooling, Microelectronics J. 31 (2000) 773–779.
[14] C.W. Leung, T.L. Chan, S.D. Probert, H.J. Kang, Forced convection from a horizontal ribbed rectangular base plate penetrated by arrays of holes, Appl. Energy 62 (1999) 81–95.
[15] R. Rachedi, S. Chikh, Enhancement of electronic cooling by insertion of foam materials, Heat Mass Transfer 37 (2001) 371–378.
[16] B.A. Jubran, S.A. Swiety, M.A. Hamdan, Convective heat transfer and pressure drop characteristics of various array configurations to simulate the cooling of electronic modules, Internat. J. Heat Mass Transfer 39 (1996) 3519–3529.
[17] C. Herman, E. Kang, Heat transfer enhancement in a grooved channel with curved vanes, Internat. J. Heat Mass Transfer 45 (2000) 3741–3757.
[18] S.V. Patankar, Numerical Heat Transfer and Fluid Flow, Hemisphere, New York, 1980.
[19] X. Chen, P. Han, A note on the solution of conjugate heat transfer problems using SIMPLE-like algorithms, Internat. J. Heat Fluid Flow 21 (2000) 463–467.